Variational quantum Monte Carlo study of charged excitons in fractional dimensional space

Troels F. Rønnow,[1,*] Thomas G. Pedersen,[1,†] Bart Partoens,[2,‡] and Kasper K. Berthelsen[3,§]
[1]*Department of Physics and Nanotechnology, Aalborg University, Skjernvej 4A, 9220 Aalborg Øst, Denmark*
[2]*Universiteit Antwerpen, Departement Fysica, Groenenborgerlaan 171, B-2020 Antwerpen, Belgium*
[3]*Department of Mathematical Sciences, Aalborg University, Frederiks Bajers Vej 7G, 9220 Aalborg Øst, Denmark*
(Received 11 February 2011; revised manuscript received 10 May 2011; published 26 July 2011)

In this article we study excitons and trions in fractional dimensional spaces using the model suggested by C. Palmer [J. Phys. A: Math. Gen. **37**, 6987 (2004)] through variational quantum Monte Carlo. We present a direct approach for estimating the exciton binding energy and discuss the von Neumann rejection- and Metropolis sampling methods. A simple variational estimate of trions is presented which shows good agreement with previous calculations done within the fractional dimensional model presented by D. R. Herrick and F. H. Stillinger [Phys. Rev. A **11**, 42 (1975) and J. Math. Phys. **18**, 1224 (1977)]. We explain the spatial physics of the positive and negative trions by investigating angular and inter-atomic distances. We then examine the wave function and explain the differences between the positive and negative trions with heavy holes. As applications of the fractional dimensional model we study three systems: First we apply the model to estimate the energy of the hydrogen molecular ion H_2^+. Then we estimate trion binding energies in GaAs-based quantum wells and we demonstrate a good agreement with other theoretical work as well as experimentally observed binding energies. Finally, we apply the results to carbon nanotubes. We find good agreement with recently observed binding energies of the positively charged trion.

DOI: 10.1103/PhysRevB.84.035316 PACS number(s): 71.35.Pq

I. INTRODUCTION

Excitons have proven to be of importance in the description of photon absorption in a wide variety of semiconducting nanostructures.[3–11] In the description of excitons and biexcitons in quasi 2D quantum wells a method widely used in literature[12–16] is based on interpolation between 1, 2, and 3 dimensions of the Laplacian and the integration measure using a single parameter D referred to as the fractional dimension. This has the great advantage that the geometrical confinement now enters through the parameter D rather than through complicated potential terms. The first study of excitons, where the confinement was modelled through a positive real number D, i.e. the fractional dimension, was done in 1991 by X. F. He[8] using the fractional dimensional model originally proposed by D. R. Herrick and F. H. Stillinger.[17] The Herrick-Stillinger model was suggested in 1975 in a study of the helium atom in noninteger dimensions. Two years later, F. H. Stillinger gave a more detailed description of the mathematical foundation of the model.[18]

We have recently reported on the binding energy of charged excitons (trions) in fractional D dimensional space[19] using the model proposed by Herrick and Stillinger. In the calculations we approximated the Hamiltonian by first removing the center-of-mass motion, expressing the Hamiltonian of relative motion in Hylleraas coordinates and finally neglecting the angle dependence of the kinetic operator. We found that the fractional D dimensional model provided accurate predictions of the trion binding energy on the surface of a cylinder.[19,20] Other authors have demonstrated that this model also predicts exciton binding energies in quantum wells and carbon nanotubes very accurately.[12–16,21] Thus, the model is applicable to a wide variety of systems.

While three-particle problems are numerically solvable within the framework of Herrick and Stillinger, the general N particle problem cannot be solved exactly within this model as it only allows two coordinates per particle, thereby restricting the maximum number of degrees of freedom. Various papers have addressed this problem in the case of biexcitons (two holes and two electrons) by assuming a square structure of the biexciton by which the Hamiltonian reduces to a two particle Hamiltonian. The resulting mathematical problem is now equivalent to that of the exciton with a different reduced mass.[7,12,22] This approximation is only applicable for biexcitons, and cannot be used for the investigation of trions, charged biexcitons, etc. Thus, in general it would be preferable to go beyond this approximation by solving the full Schrödinger equation. Recently, C. Palmer and P. N. Stavinou suggested a more general model within which the Herrick-Stillinger model is contained.[23] Contrary to the Herrick-Stillinger model, the Palmer model allows one to introduce M coordinates describing the position of each particle. Although the foundation for solving N particle problems has been established with this work, the model has only received very little attention,[24–28] and moreover, it has not yet been applied to any three-particle problems containing Coulomb interactions between all three particles.

The quantum Monte Carlo (QMC) method has proven to be a powerful tool to estimate as well as to find exact solutions to excitonic problems.[29–31] The simplest form of QMC is variational quantum Monte Carlo (VQMC) which, to our knowledge, has not yet been applied to fractional dimensional systems neither using the Herrick-Stillinger model nor the Palmer model. In VQMC one tries to sample a distribution $\rho(x) \geqslant 0$, where x denotes all particle coordinates $\vec{r}_1 \ldots \vec{r}_N$ for N particles, with an ensemble of walkers. Using the sampled configurations one can estimate integrals of the form $\langle E \rangle = \int \rho(x) E_L(x) dx$ with a sum $\langle E \rangle \approx \sum_i E_L(x_i)/P$, where P is the number of sampling points. The most common quantity estimated is the expectation value of the energy

for which one defines the local energy as $E_L = \Psi^{-1}\hat{H}\Psi$, where Ψ is a trial function and $\hat{H}$ is the Hamilton operator. It is important to gain a basic understanding of how VQMC is carried out in fractional dimensional systems as it provides the basis for more complicated approaches such as Fokker-Planck VQMC and diffusion QMC. One obvious complication though is the singularities occurring in the integration measure. While the integration measure is finite for one-particle systems whenever the dimension $D \geqslant 1$, the problem complicates for more particles. In general for N particles each living in a fractional D dimensional space, the integration measure turns out to be singular whenever $D < N - 1$, in cases where the center-of-mass motion can be separated out.[23] In a VQMC study, these singularities should either be included in the local energy or in the probability distribution which in itself constitutes a challenge as one would like, on the one hand, the local energy E_L to be slowly varying and, on the other hand, still be able to evaluate the fraction of the probability distribution at two distinct points[32] $\rho(x)/\rho(x')$.

In this article, we investigate excitons and trions using variational estimates based on VQMC in fractional dimensional space using the Palmer model. This article aims toward (1) explaining how to carry out VQMC for fractional dimensional systems, and (2) demonstrating the some applications of this model. In Sec. II, we present the necessary integration measure. For excitons we present a direct method for generating random numbers reproducing the probability distributions of a family of trial functions containing the exact solution. We suggest a variational wave function for the trion which we use to estimate the trion binding energies through VQMC. Using the established theory we present binding energies of the fractional dimensional excitons in Sec. III, which we compare with the exact result. The trion binding energy is presented in Sec. IV, where we compare the results with the results in Ref. 19. We then investigate the energy dependence on the collapse of the axes within the framework of Palmer and study the trion wave functions and their dependence on the dimension of the system. As an application of this model we study three systems: (1) we estimate the hydrogen molecular ion in two- and three dimensions, (2) we study trions in GaAs-based quantum wells, and (3) we apply the model to estimate the binding energy of positively charged trions in carbon nanotubes (CNTs). The results are compared with the recently measured trion binding energies in Ref. 33.

II. THEORY

We will use phrases such as "fractional dimensional space" with "dimension" D. The "dimension" D should not be confused with the mathematical dimension N of the space $\mathbb{R}^N$. Likewise, the "fractional dimensional space" refers to the interpolations applied to the Laplacian and the integration measure rather than $\mathbb{R}^N$. In our case all calculations are carried out in $\mathbb{R}^{3N}$, where $N + 1$ is the number of particles. For completeness and to fix the notation, we provide a brief review of the Palmer- and Herrick-Stillinger models in Appendix A. We will use the result Eq. (A9)

$$\int f(x)dx = \sigma^N(D-1) \times \int_0^\infty \int_0^{2\pi} \cdots \int_0^\infty \int_0^{2\pi} f(r_1,\theta_1,\ldots,r_N,\theta_N) \times \prod_j^N r_j^{D-1} |\sin\theta_j|^{D-2} dr_j d\theta_j, \quad (1)$$

to derive a direct method to calculate the exciton-binding energy, but in general, our calculations will be based on the Palmer model using Cartesian coordinates with the weighted integration defined in Eq. (A5),

$$\int f(x)dx = \sigma^N(\alpha)\sigma^N(\beta)\sigma^N(\gamma) \int_{-\infty}^\infty \cdots \int_{-\infty}^\infty f(\vec{r}_1,\ldots,\vec{r}_N) \times \prod_{i=1}^N |x_i|^{\alpha-1}|y_i|^{\beta-1}|z_i|^{\gamma-1} dx_i dy_i dz_i. \quad (2)$$

The parameter D in Eq. (1) is defined as the sum $D = \alpha + \beta + \gamma$. It is worth noting that D, widely used in literature,[7,8,12,19,21,22] is not uniquely determined as, for instance, $\alpha = 1$, $\beta = 1$, $\gamma = 0.5$, and $\alpha = 0.75$, $\beta = 0.8$, $\gamma = 0.95$ would yield the same D. This was also noted in Ref. 23, and thus, a statement as[19] "Carbon nanotubes are effectively $D \approx 1.71$ nanostructures" is in general not very precise as it provides no information about which axes are collapsed and which are not. In some special cases, however, one parameter D is sufficient, as the problem becomes independent of the choice of α, β, and γ. We will discuss this subject in Sec. IV.

A. Excitons

In the case of a single hole and a single electron, the D dimensional Hamiltonian can be shown to give[8]

$$\hat{H}_X = -\frac{\partial^2}{\partial r^2} - \frac{D-1}{r}\frac{\partial}{\partial r} + \frac{\hat{l}^2}{r^2} - \frac{2}{r}, \quad (3)$$

with

$$\hat{l}^2 = -\frac{1}{\sin^{D-2}\theta}\frac{\partial}{\partial\theta}\sin^{D-2}\theta\frac{\partial}{\partial\theta}, \quad (4)$$

after removal of the center-of-mass motion when distances are expressed in effective Bohr radii a_B^* and energies in effective Rydbergs Ry^*. These quantities are material-dependent parameters defined by the dielectric constant ε and the electron- and hole masses m_e and m_h through the reduced mass $\mu = m_e m_h/(m_e + m_h)$. By definition $a_B^* = 0.529\,\text{Å} \cdot \varepsilon/\mu$ and $Ry^* = 13.6\,\text{eV} \cdot \mu/\varepsilon^2$. In the following, we will study the ground state of the Wannier equation and will therefore assume that the wave function is independent of the angle θ. Using an exponential trial function $\Psi(r) = e^{-ar}$ the local energy is

$$E_L(r) = -a^2 + a\frac{D-1}{r} - \frac{2}{r}, \quad (5)$$

for configurations distributed with the probability distribution $\rho(r) = Ae^{-2ar}r^{D-1}$, with A being a normalization constant. Using this distribution, the energy can be estimated as

$$E_X \approx \frac{1}{N}\sum_{i=1}^{N} E_L(r_i), \tag{6}$$

where the distance r_i can be generated by

$$r_i(p_i) = \frac{Q^{-1}(D,p_i)}{2a}, \tag{7}$$

using random numbers p_i distributed uniformly on the interval $[0,1]$. Here $Q^{-1}(x,y)$ denotes the inverse regularized gamma function defined as the inverse of the function

$$Q(a,z) = \frac{1}{\Gamma(a)}\int_z^\infty t^{a-1}e^{-t}dt. \tag{8}$$

This result is easily derived within the framework of Herrick and Stillinger using the integration in Eq. (1). Obviously, the local energy is constant when $a = 2/(D-1)$, which demonstrates that the exact ground state is in the variational function space. In the following, we define the exciton binding energy as $-E_X$, where E_X is the ground state energy of the Hamiltonian given in Eq. (3).

B. Trions

For trions the radial part of the Hamiltonian can be shown to give,[19]

$$\begin{aligned}\hat{H}_T = &-\frac{\partial^2}{\partial r_{12}^2} - \frac{\partial^2}{\partial r_{13}^2} - \frac{2}{\sigma+1}\frac{\partial^2}{\partial r_{23}^2}\\ &-\frac{\sigma}{\sigma+1}\frac{r_{12}^2+r_{13}^2-r_{23}^2}{r_{12}r_{13}}\frac{\partial^2}{\partial r_{13}\partial r_{12}} - \frac{2(D-1)}{r_{23}(\sigma+1)}\frac{\partial}{\partial r_{23}}\\ &-\frac{r_{12}^2+r_{23}^2-r_{13}^2}{(1+\sigma)r_{12}r_{23}}\frac{\partial^2}{\partial r_{12}\partial r_{23}} - \frac{(D-1)}{r_{12}}\frac{\partial}{\partial r_{12}}\\ &-\frac{r_{13}^2+r_{23}^2-r_{12}^2}{(1+\sigma)r_{13}r_{23}}\frac{\partial^2}{\partial r_{13}\partial r_{23}} - \frac{(D-1)}{r_{13}}\frac{\partial}{\partial r_{13}}\\ &-\frac{2}{r_{13}} - \frac{2}{r_{12}} + \frac{2}{r_{23}},\end{aligned} \tag{9}$$

where $\sigma = m_e/m_h$ is the mass fraction between the electron- and hole masses. Because the two electrons (two holes) must obey the Fermi-Dirac statistics the total wave function must be antisymmetric under exchange of the two particles. In this work we will only be concerned with trions having antisymmetry in the spin part, i.e. singlet trions. We will therefore assume that the solution to Eq. (9) is symmetric in the spatial part. In our previous work we found that variational estimates of negative trions should be created from wave functions that can model an exciton with a weakly bound electron.[19] This, unfortunately, indicates that the variational estimates, which have proven great successes within the helium atom, are not necessarily good estimates for trions since the magnitude of the hole charge in trions is one-half of the nuclear charge of helium. On the contrary, for the positively charged hydrogen molecule H_2^+ all particle charges are of magnitude one and, thus, its properties are expected to be much like those of the positive trion. Inspired by variational estimates[34] of H_2^+ along with the conclusions from Ref. 19, we chose a trial wave function of the form

$$\begin{aligned}\Psi_T(r_{12},r_{13},r_{23}) = &A\Psi_H(r_{12},r_{13})\\ &\times \exp\left(\frac{\sigma+1}{D-1}\frac{r_{23}}{1+br_{23}+cr_{23}^2}\right),\end{aligned} \tag{10}$$

with

$$\begin{aligned}\Psi_H(r_{12},r_{13}) = &\exp\left[\frac{-2a(r_{12}+\eta r_{13})}{D-1}\right]\\ &+\exp\left[-\frac{2a(\eta r_{12}+r_{13})}{D-1}\right],\end{aligned} \tag{11}$$

being the Hylleraas-Eckart-Chandrasekhar trial function and where A is a normalization constant.[17,19] Here $a,b,c \in \mathbb{R}$, and $\eta \in [0,1]$ are variational parameters. In the same manner as with the exciton, the local energy E_L was found[35] for probability distributions $\rho(\vec{r}_{12},\vec{r}_{13})$ which include the integration weight of Eq. (2)

$$\rho = |\Psi_T|^2|x_{12}|^{\alpha-1}|y_{12}|^{\beta-1}|z_{12}|^{\gamma-1}|x_{13}|^{\alpha-1}|y_{13}|^{\beta-1}|z_{13}|^{\gamma-1}.$$

The inclusion of the integration weight is a necessity to ensure that the local energy is varying sufficiently slowly. Here we have omitted the dependence of ρ and Ψ_T on $\vec{r}_{12}$ and $\vec{r}_{13}$ for brevity. Throughout this article we denote the trion energy with E_T, and moreover, we define the trion binding energy as the quantity $E_X - E_T$, which is positive for stable trions. Also, we will denote the trion states by S_σ^+ and S_σ^- for the positive and negative singlet trion with mass fraction σ, respectively. Finally, the wave functions will be denoted $|S_\sigma^+\rangle$ and $|S_\sigma^-\rangle$.

III. EXCITON-BINDING ENERGY

In this section, we present results on fractional dimensional exciton using three different methods: (I) using a Metropolis algorithm, (II) using a von Neumann rejection algorithm, and, (III) using the analytical expression in Eq. (7). For comparison purposes we also give the exact expectation value for trial functions of the form $\Psi(r) = e^{-ar}$,

$$\frac{\langle\Psi|\hat{H}|\Psi\rangle}{\langle\Psi|\Psi\rangle} = a\left(a - \frac{4}{d-1}\right). \tag{12}$$

While the sampling process using the von Neumann rejection algorithm and Eq. (7) produce uncorrelated data, the Metropolis algorithm does not necessarily generate uncorrelated sampling points. In order to avoid correlation between data points 50 accept/reject cycles were performed in between each sample. Moreover, to ensure that the samples were uncorrelated we calculated the auto correlation function for a single walker[36]

$$A(l) = \frac{1}{\Sigma^2 N}\sum_{i=0}^{N-l}[E_L(x_i) - \langle E\rangle][E_L(x_{i+l}) - \langle E\rangle], \tag{13}$$

where $\langle E\rangle$ is the mean value of $\{E_L(x_i)\}$, N is the number of sampling points, x_i is the i'th sampled configuration, Σ^2 is the variance with the standard deviation Σ defined as

$$\Sigma = \sqrt{\frac{1}{N}\sum_{i=1}^{N}[E_L(x_i) - \langle E\rangle]^2}, \tag{14}$$

and l is the lag. In all cases examined we found no signs of correlation of the sampled energies. For all calculations presented in this paper we calculated the standard deviation Σ of the sampling which is indicated in the figures with error bars. The von Neumann rejection algorithm was carried out by selecting random numbers in a "D dimensional box", i.e., with a distribution $\propto |x|^{\alpha-1}|y|^{\beta-1}|z|^{\gamma-1}$, with side lengths L and then accepting the sampled configuration according to the fraction $|\Psi(r)|^2/c$, where $c = \max_{r\in\mathbb{R}} |\Psi(r)|^2$. The distribution of the D dimensional box can be sampled directly by first calculating x, y, and z according to

$$x = s_x L p_x^{\frac{1}{\alpha}}, y = s_y L p_y^{\frac{1}{\beta}}, \text{and} z = s_z L p_z^{\frac{1}{\gamma}}, \tag{15}$$

where p_x, p_y, and p_z are uniformly distributed numbers on the interval $[0,1]$, s_x, s_y, and $s_z \in \{-1,1\}$ are random discrete numbers and then calculating $r = \sqrt{x^2+y^2+z^2}$ in $\mathbb{R}^3$. The Metropolis algorithm was implemented in a straightforward manner as explained in Ref. 32. All Metropolis calculations were carried out with acceptance rates between 70% and 90%, and all proposed walks were found using normally-distributed random numbers.

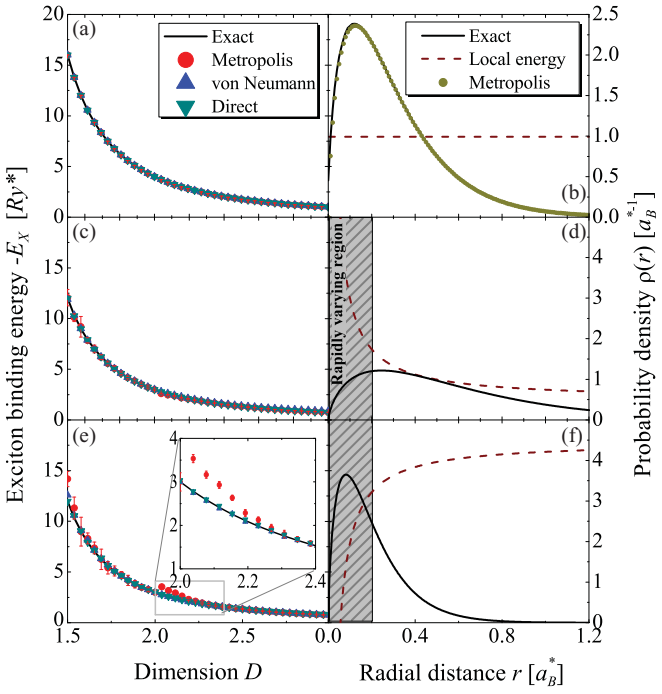

FIG. 1. (Color online) Exciton binding energies calculated using VQMC with $\Psi = e^{-ar}$ for different a's. In a, c, and e the binding energies $\langle\Psi|\hat{H}|\Psi\rangle/\langle\Psi|\Psi\rangle$ are calculated for $a = 2/(D-1)$, $a = 1/(D-1)$ and $a = 3/(D-1)$, respectively. Four curves are presented: Four curves are presented: (I) a Metropolis calculation, (II) a von Neumann calculation, and, (III) a calculation based on Eq. (5) and the distribution generated by Eq. (7), and the solid line (Exact) is the exact analytical expression for the expectation value Eq. (12). In b, d, and f the local energies and exact probability distributions are given for the three cases: $a = 2/(D-1)$, $a = 1/(D-1)$and $a = 3/(D-1)$. Additionally in b, we have given the probability distribution obtained from our Metropolis algorithm. The illustrations as well as calculations in b, d, and f were made for $D = 1.7$.

As shown in Fig. 1(a) the agreement between the three methods (I)-(III) and Eq. (12) is excellent. This is not surprising as the local energy is constant in the case where $a = 2/(D-1)$. This means that one can not conclude that the algorithm has been correctly implemented by just looking at the expectation value of energy in this special case. Thus, to ensure that the probability distribution was correctly sampled, we checked the sampled probability distribution against the analytical one (Fig. 1(b)) and found good agreement between the two.

To further test the implementation we also investigated cases using wave functions different from the exact solution by letting $a = g/(D-1)$, with $g = 1$ or $g = 3$ Figs. 1(c) and 1(e). Again we found good agreement between Eq. (12) and the three different implementations (I)-(III). However, one remarkable thing is the failure of the Metropolis algorithm for D slightly larger than 2 in. Fig. 1(e) This failure is caused by two issues. To understand the first issue we have plotted the local energy along with the exact analytical probability distribution $\rho(x,y,z) = \Psi^2(r)|x|^{\alpha-1}|y|^{\beta-1}|z|^{\gamma-1}$ for two cases of g, see Figs. 1(d) and 1(f). In the first case, $g = 1$, the local energy remains nearly constant[37] in the region where $r > 0.2a_B^*$ and the accumulated probability distribution is small for $r < 0.2a_B^*$. This means that small inaccuracies in the sampling process only will yield a small error, and thus, we still get close to the exact result. In the second case, $g = 3$, the local energy also remains constant for $r > 0.2a_B^*$ and varies rapidly for r below $0.2a_B^*$. However, in this case the accumulated probability distribution is large for $r < 0.2a_B^*$ and thus, small inaccuracies yield large errors. The second issue is related to the sampling process in the Metropolis algorithm and is caused by the singularity of the probability distribution $\rho(x,y,z)$. When an axis is collapsed the function $\rho(x,y,z)$ becomes more and more singular due to the integration weight $|z|^{\gamma-1}$. This means that when γ becomes small the walkers must be moved with extremely small steps if one wants the transition probability to be non-zero. This explains why the error only occurs for the Metropolis algorithm, while implementation II and III yield exact energies; they do not depend on fractions involving walker positions. Thus, to cure this problem one has to increase the number of sampling steps and to decrease the mean variance of each proposed walk. We have found that to prevent this issue from arising it is useful to scale the mean variance of the random movement according to the dimension of each of the axes, i.e., Δx according to α, Δy according to β and Δz according to γ.

Finally, a few points are worth noting: First of all, we see that, while the variance increases as $|g-2|$ grows, the agreement with the exact result is still extremely good. Secondly, the variance increases with decreasing dimension in general. This is easy to understand; the two particles are more confined for low dimensions than for high dimensions and thereby the Coulomb interaction becomes more significant with decreasing D meaning that the singularity in the local energy plays a more important role. It is also worth mentioning that we have found that the Metropolis algorithm is much faster than the von Neumann algorithm. The reason for this is that the von Neumann guesses, inside a D dimensional box, in general have a high rejection rate as these do not come close to the exponential behavior of the wave function. However, the method has the benefit that one gets rid of the singular behavior

of the probability distribution, which makes it extremely easy to implement. The Metropolis algorithm, however, is based on fractions, in which both denominator and numerator may attain the values 0 and ∞. Therefore one has to take care that the actual implementation is done carefully such that these special cases are handled correctly. In conclusion the von Neumann rejection algorithm serves as a good algorithm for reproducing and checking results obtained using the Metropolis algorithm, but is not recommended for large calculations.

IV. TRION BINDING ENERGY

To obtain a minimal energy with respect to the variational coefficients a damped steepest decent method was implemented using the stochastic gradient approximation[38,39]

$$a_{j+1} = a_j - \frac{2\xi_j}{N}\left[\sum_i^N \frac{\Psi_T'(x_i)}{\Psi_T(x_i)} E_L(x_i) - \langle E\rangle \sum_i^N \frac{\Psi_T'(x_i)}{\Psi_T(x_i)}\right],$$

where $\Psi_T(x)$ is the trial function, $\Psi_T'(x)$ is the derivative of the trial function with respect to a, x_i is the i'th configuration, N is the number of sampling points, a_j is the coefficient at iteration j, a_{j+1} is the new coefficient at iteration $j+1$, ξ_j is a damping coefficient, and $\langle E_L\rangle$ is the expectation value of the energy in the overall sampling. The damping coefficient was chosen as $\xi_j = q/j^p$ in accordance with the considerations on the convergence in Ref. 38. Rather than optimising the parameters for every calculation we used this method to minimize the energy for selected points. In between these points the parameters were estimated using appropriate interpolations. For each optimisation we chose $p \in [0.8,1]$ and $q \in [0.05,2]$, and every optimization was carried out several times with different p and q. Many different starting points were used for each set of coefficients to ensure that the coefficients found were the best possible. Moreover, every optimized point was thoroughly tested with different number of sampling points to guarantee that the minimum found was not caused by an insufficient set of sampling points.

We calculated trion binding energies with the Palmer integration for the negative trion $S^-_{0.0}$, the positive trion $S^+_{0.0}$ and the trion $S^{+/-}_{1.0}$, for which the energies of the negative and positive trions coincide. In Fig. 2 it is seen that the agreement between the results presented here and those in Ref. 19 is extremely good. Thus, our simple trial function in Eq. (10) resembles the properties of the $S^-_{0.0}$ and $S^{+/-}_{1.0}$ trions with good accuracy. It is seen that the variance of the integration becomes much larger as the dimension is decreased as we also saw for the exciton. Moreover, the $S^+_{0.0}$ is in general much stronger bound than the $S^{+/-}_{1.0}$ and $S^-_{0.0}$. This means that in general we would expect the $S^+_{0.0}$ to be much more localized than both $S^{+/-}_{1.0}$ and $S^-_{0.0}$.

Also, the mass fraction dependence was compared with the results in Ref. 19. As shown in Fig. 3 there is a very good agreement with the approach presented here and the results obtained in Ref. 19. Whereas the negative trion comes very close to the result in Ref. 19, the positive trion is slightly more inaccurate. However, the mass fraction spectrum demonstrates that the variational estimate presented here covers a large class of different physical systems varying from the H_2^+ structure to the He atom with nuclear charge 1. In terms of the ground state energy E_T the general error of this estimate is less than 2.5%. Hence, essential properties of this wave function, such as expectation values of the electron-hole and electron-electron distances, are expected to be predicted with high accuracy.

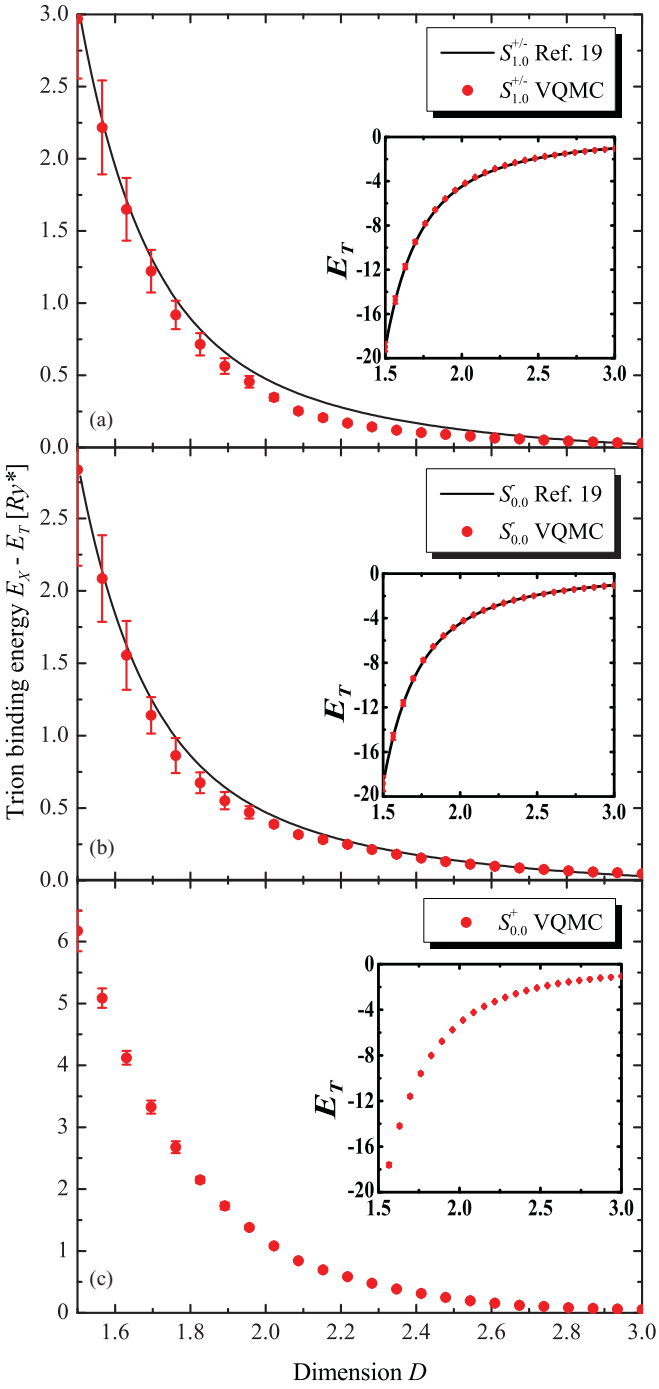

FIG. 2. (Color online) Trion binding energy for a) $S^{\pm}_{1.0}$, b) $S^-_{0.0}$ and c) $S^+_{0.0}$ trion using VQMC and a basis expansion. The basis expansion was carried out as done in Ref. 19 within the Herrick-Stillinger framework. The VQMC binding energy was found using the Palmer model[23] with collapse of one axis at a time, first z and then y. Inset: The lowest eigenvalues E_T of the respective Hamiltonians.

With reference to the comments made in Sec. II the dimensional parameters α, β, and γ are not uniquely determined

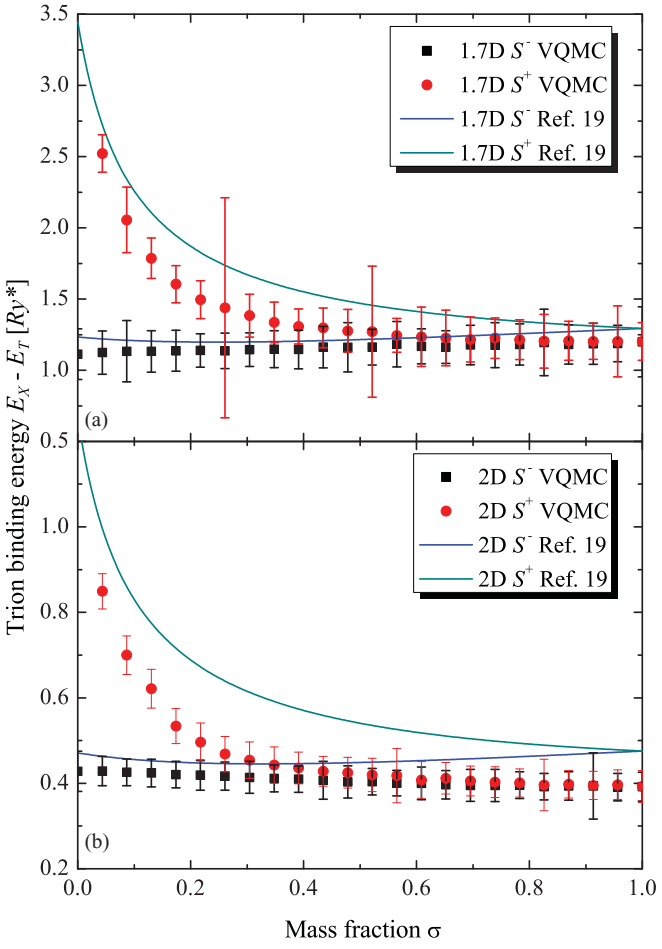

FIG. 3. (Color online) Trion binding energies $E_X - E_T$ for S^+_σ and S^-_σ trions using VQMC for the wave function in Eq. (10) and the basis expansion given in Ref. 19. In (a) we give the binding energies for $D = 1.7$, and (b) for $D = 2$.

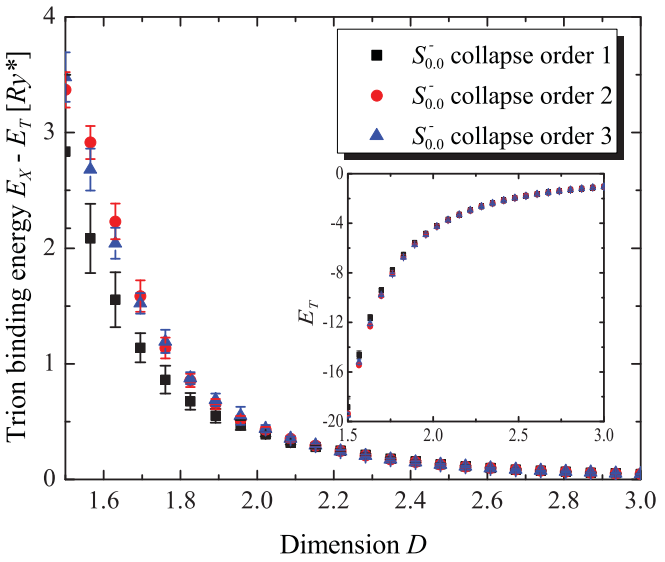

FIG. 4. (Color online) Trion binding energy for $S^-_{0.0}$ trion versus the dimension $D = \alpha + \beta + \gamma$ for different collapse orders. Collapse order 1, first we collapse the z-axis and then the y-axis. Collapse order 2, all collapse parameters were set to $D/3$. Collapse order 3, we kept $\alpha = 1$ and set $\beta = \gamma = (D - 1)/2$. The small deviation between the different ways of collapsing the axes is ascribed to the sampling of the singularities as illustrated in Fig. 1.

by the dimension D, and so there is no guarantee that the energy is independent of the choice of these parameters for a constant $D = \alpha + \beta + \gamma$. In Fig. 4, we have plotted the binding energy as a function dimension D for different ways of collapsing of the axes: First we collapsed the axes one by one starting with z by letting γ go from 1 to 0 and then collapsing y, by letting β decrease from 1. We then collapsed the axes simultaneously $\alpha = \beta = \gamma = D/3$ for $D \in [1.5,3]$, and finally we kept one axis fixed $\alpha = 1$ collapsing the two remaining axes simultaneously $\beta = \gamma = (D - 1)/2$. At first sight, one might be led to believe that there is a difference between the different ways of collapsing the axes. But, this can clearly not be the case for our system: First of all, it is evident that for $\alpha = 1$, $\beta = 1$ or $\gamma = 1$ the expectation value is independent of choice of the remaining parameters for any $D = \alpha + \beta + \gamma$. This is a direct consequence of the discussion in Appendix A meaning that for collapse order 1 and 3 the energy difference can be shown to be identical mathematically. However, one would expect that the error bars would overlap, which is clearly not the case. This can be explained in terms of the singular behavior of the probability distribution: When using collapse order 3 the singularities are much more dominant as the distribution becomes singular in two coordinates per particle which leads to higher numerical errors in the energy. As the singularities imply smaller steps, as discussed earlier, the variance becomes smaller. In this context it is important to stress that the variance does not include the numerical inaccuracy arising from the singularities. Secondly, the Hamiltonian in Eq. (9) depends only on D. This means that the exact eigenfunctions as well as energies also only depend on D. Therefore, for any trial function that can be expressed as a linear combination of the eigenfunctions to the Hamilton operator Eq. (9) the expectation value of the energy will only depend on D rather than α, β, and γ. However, if one included the angular dependence into the trial function and the Hamilton operator Eq. (9) this would no longer be the case: One would need two independent collapse parameters[40] to describe the dimension of the system Eq. (9). In conclusion, to get the most reliable results one should choose a collapse order for which the least singularities occur, i.e., collapsing one axis at a time. Throughout the rest of this paper we collapse one axis at a time starting with the z-axis and then the y-axis.

One of the major advantages of the approach presented in this article is our simple wave function. Unlike the method in Ref. 19, where the wave function consists of more than 180 terms, one can easily perform numerical integration of the wave function presented here. We estimated the expectation values $\langle S_\sigma|r_{12}|S_\sigma\rangle$, $\langle S_\sigma|r_{13}|S_\sigma\rangle$, $\langle S_\sigma|r_{23}|S_\sigma\rangle$, and $\langle S_\sigma|\theta_{23}|S_\sigma\rangle$ to gain an insight into the structure of the wave function.

The results are shown in Fig. 5. Several interesting things are seen: First of all, it is immediately seen that all distances on average become smaller as the dimension is decreased. This is also what we would intuitively expect, since an increased confinement should yield smaller expectation values of the distances. Secondly, the $S^{+/-}_{1.0}$ and the $S^-_{0.0}$ are very similar

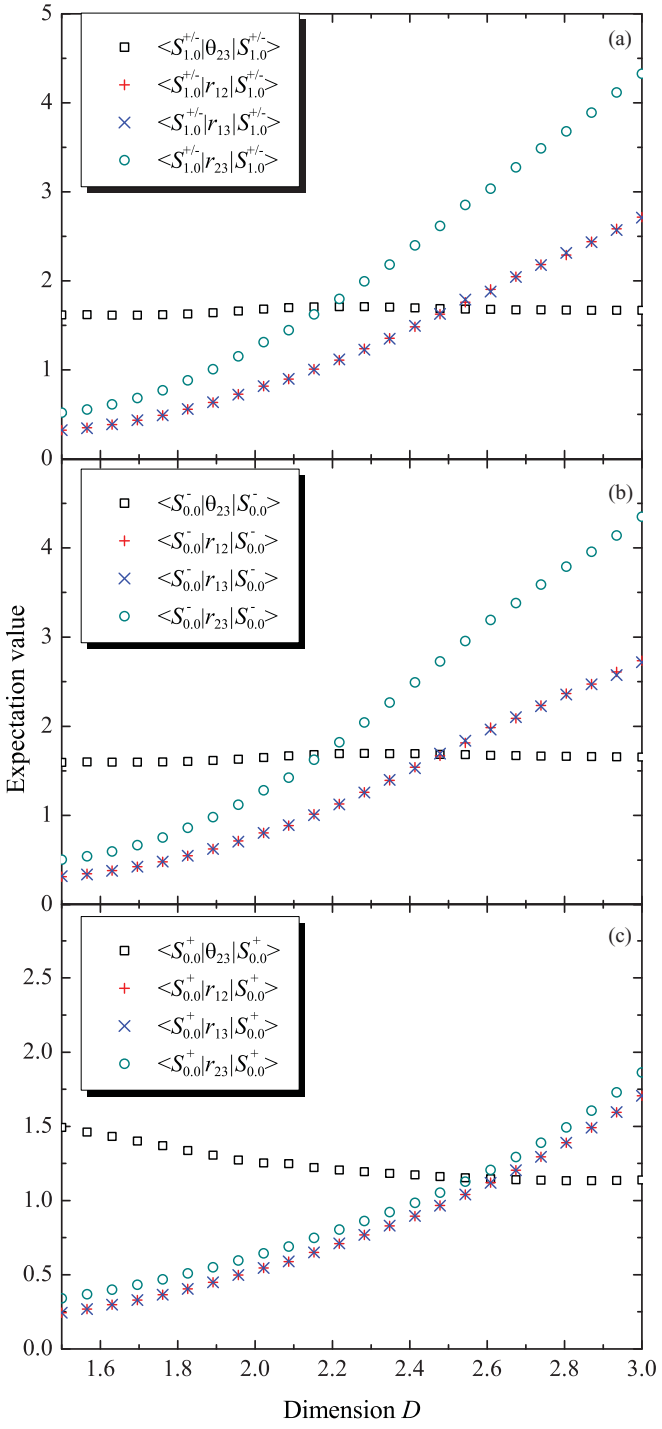

FIG. 5. (Color online) Expectation values of r_{12}, r_{13},r_{23}, and θ_{23} as a function of dimension D for a) $S^{+/-}_{1.0}$, b) $S^{-}_{0.0}$, and c) $S^{+}_{0.0}$.

with regards to energy (see Fig. 2 and Fig. 3) as well as to the average distances and angles in Figs. 5(a) and 5(b) meaning that the $S^{-}_{0.0}$ wave function is expected to have very similar properties to that of $S^{+/-}_{1.0}$. On the contrary, the average distances for $S^{+}_{0.0}$ are much smaller than those of $S^{-}_{0.0}$. In general we would expect $S^{+}_{0.0}$ to be more localized than $S^{-}_{0.0}$ which is good agreement with the higher binding energy for $S^{+}_{0.0}$. Another major difference is that for $S^{+}_{0.0}$ the average distances $\langle S^{+}_{0}|r_{12}|S^{+}_{0}\rangle$, $\langle S^{+}_{0}|r_{13}|S^{+}_{0}\rangle$, and $\langle S^{+}_{0}|r_{23}|S^{+}_{0}\rangle$ are almost equal. This means that the two holes are closer to each other in comparison with $S^{-}_{0.0}$ thereby lowering the average angular difference $\langle S^{+}_{0.0}|\theta_{23}|S^{+}_{0.0}\rangle$ which indeed is what is seen. Third, it is seen that the distance expectation values to a large extent exhibits a linear behavior on the interval $D \in [2,3]$. This is not so surprising as a similar tendency is seen for the exciton: If one scales the distances with $2/(D-1)$ and the energy with $(D-1)^2/4$ one finds the wave function and Hamiltonian[17] to be independent of D meaning that for excitons one finds that the expectation value of $\langle X|r_{12}|X\rangle$, $\langle X|r_{13}|X\rangle$, and $\langle X|r_{23}|X\rangle$ scales as $D-1$.

Finally, the average angular difference[41] $\langle S_\sigma|\theta_{23}|S_\sigma\rangle$ between the electron-hole directions for $S^{-}_{0.0}$ and $S^{+/-}_{1.0}$, varying from 1.60 for $D=1.5$ to 1.65 for $D=3$ for $\sigma=0$, are slowly growing as D is increased. If one completely neglects the correlation of the wave function, i.e., assume that it would simply be a product of two excitonic orbitals, the expectation value of the average angular difference can be found to be $\pi/2$ on the interval[42] $D \in [1.5,3]$. This angle is slightly smaller then the true expectation value given in Fig. 5 demonstrating that the average angular difference is increased as a result of correlation effects. The correlation effects are most pronounced for large D which is in agreement with the conclusions in Ref. 19, where it was shown that the fraction between correlation energy and the full energy increases with increasing dimension. The $S^{+}_{0.0}$ state is again different in comparison with $S^{-}_{0.0}$. For $S^{+}_{0.0}$ the average angular difference $\langle S^{+}_{0.0}|\theta_{23}|S^{+}_{0.0}\rangle$ varies from 1.38 at $D=1.5$ to 1.05 at $D=3$. This means that one would expect that the probability of finding the electron in between the two holes is lower than finding the electron with a large distance to both holes in agreement with what is seen for the ionised hydrogen molecule.[34] This is also the reason why all average distances are equal.

We also investigated the probability distributions

$$\rho_r(r_1,r_2) = \int_0^{2\pi}\int_0^{2\pi} |\Psi_T(r_1,r_2,\theta_1,\theta_2)|^2 \times r_1^{D-1} r_2^{D-1} |\sin\theta_1|^{D-2} |\sin\theta_2|^{D-2} d\theta_1 d\theta_2, \quad (16)$$

and

$$\rho_\theta(\theta_1,\theta_2) = \int_0^{\infty}\int_0^{\infty} |\Psi_T(r_1,r_2,\theta_1,\theta_2)|^2 \times r_1^{D-1} r_2^{D-1} |\sin\theta_1|^{D-2} |\sin\theta_2|^{D-2} dr_1 dr_2. \quad (17)$$

In the case of $S^{-}_{0.0}$ ($S^{+}_{0.0}$) the probability distribution Eq. (16) gives the probability $\rho_r(r_1,r_2)dr_1dr_2$ of finding one electron (hole) with distance between r_1 and r_1+dr_1 and the other electron (hole) with distance between r_2 and r_2+dr_2. Likewise, Eq. (17) gives the probability $\rho_\theta(\theta_1,\theta_2)d\theta_1 d\theta_2$ of finding an electron (hole) with an angle between θ_1 and $\theta_1+d\theta_1$ from the x-axis, in the plane spanned by the trion, and finding the other electron (hole) with angle between θ_2 and $\theta_2+d\theta_2$.

We have plotted four different radial probability distributions for $S^{-}_{0.0}$ in Fig. 6 with $\sigma=0$ and a) $D=3.0$, b) $D=2.5$, c) $D=2.0$, and d) $D=1.7$. First we notice that the probability distributions contract as the dimension D decreases, in agreement with the results in Fig. 5. The shapes of the wave functions are more or less the same independent of D. Again this can be explained by examining the exciton: If

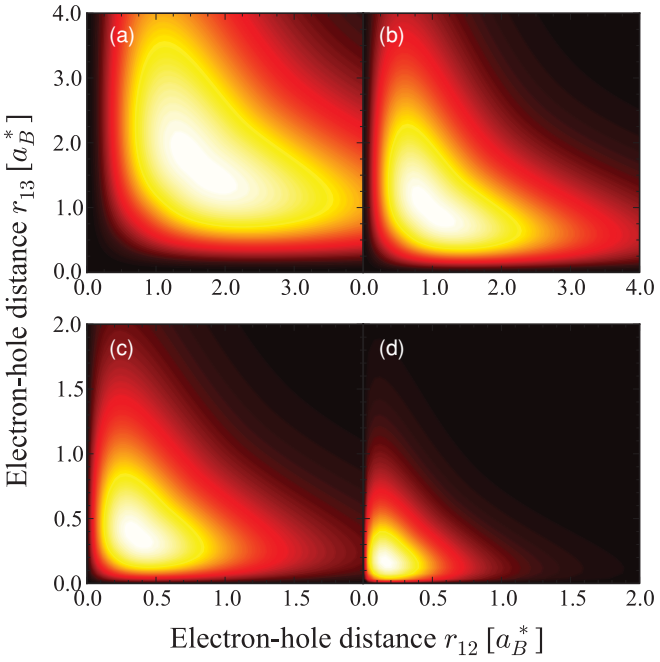

FIG. 6. (Color online) Radial probability distribution ρ_r (Eq. (16)) for the $S_{0.0}^-$ state for different dimensions D: a) $D = 3.0$, b) $D = 2.5$, c) $D = 2.0$, and d) $D = 1.7$.

one scales distances and energies of the exciton, as explained in previous paragraphs, the wave function becomes independent of D. Hence, the shapes of the exciton wave functions are exactly the same for any dimension D. In general, the $S_{0.0}^-$ wave function has the shape of a butterfly wing with high

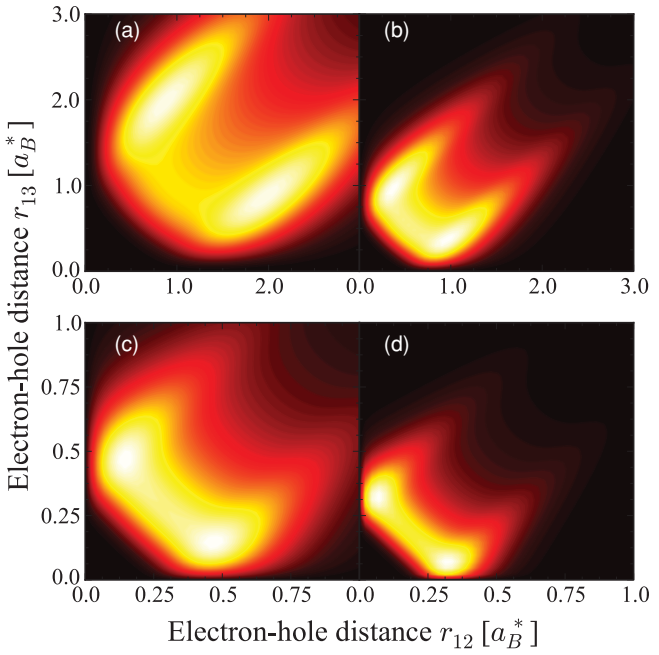

FIG. 7. (Color online) Radial probability distribution for the positively charged heavy hole trion $S_{0.0}^+$ for a) $D = 3.0$, b) $D = 2.5$, c) $D = 2.0$, and d) $D = 1.7$. In comparison with Fig. 7 these distributions are much more localized. One very interesting feature is the local maximum along the line $r_2 = r_1 + k$ where $k \approx 1a_B^*$. This shows that the electron with high probability can be found near one of the two holes.

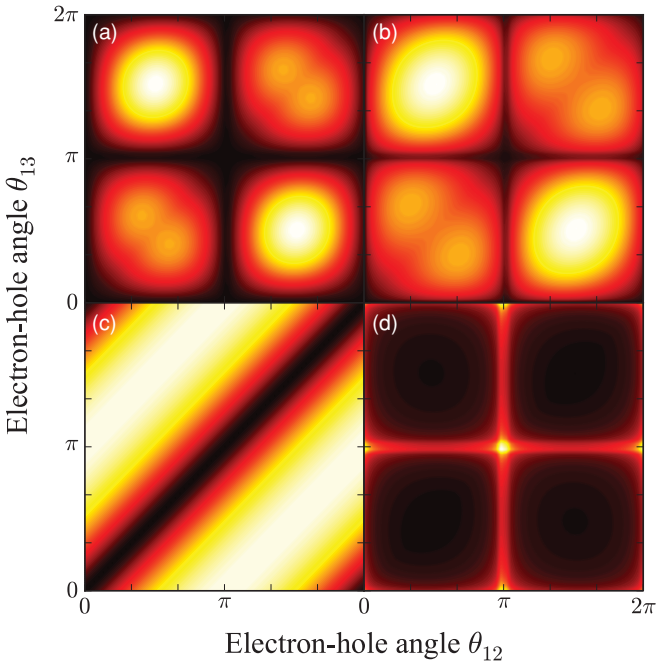

FIG. 8. (Color online) Probability distribution ρ_θ for $S_{0.0}^-$ as function of angles θ_{12} and θ_{13} for a) $D = 3.0$, b) $D = 2.5$, c) $D = 2.0$, and d) $D = 1.7$. The definition of ρ_θ is given in Eq. (17). Notice the pattern along the line $\theta_{13} = \theta_{12}$ as well as the local minimum. This is a result of electron-electron repulsion and it is responsible for the expectation value $\langle S_{0.0}^-|\theta_{23}|S_{0.0}^-\rangle$ being slightly larger than $\pi/2$.

probabilities of finding one electron close to the hole whenever the other electron is far away from the hole. This clearly demonstrates that the wave function is a superposition of two excitons, formed by the first and second electron bound to the hole, respectively, each weakly bound to the remaining electron. We have plotted the radial probability distribution in Fig. 7 for $S_{0.0}^+$. It is seen that the $S_{0.0}^+$ state is, in general, more localized than the $S_{0.0}^-$ and that the shape of the wave function is very different. One very interesting feature is the two maxima near the lines $r_2 = r_1 \pm k$, where $k \approx 1a_B^*$ for $D = 3$. This suggests that with high probability one will find the electron near one hole-site and that the probability of finding the electron in between the two holes is much smaller, which is in good agreement with our previous conclusions.

Next, we investigated the angular distribution in Eq. (17) which has been shown for the case of $\sigma = 0$ in Fig. 8. We immediately notice the pattern stretching the wave function along the direction $\theta_{13} = \theta_{12}$. This effect arises from the correlation and is simply a consequence of the electron-electron repulsion: It is clearly seen that the angular differences θ_{23} near π are favored over angular differences near 0, though this effect is subtle. This means that the probability of finding the two electrons close to each other, in general, will be smaller than the probability of finding them separated by an angle of π in agreement with our former discussion of the expectation value of θ_{23}. Finally we plotted the angular distribution for $S_{0.0}^+$, (Fig. 9). Again a pattern is seen along $\theta_{13} = \theta_{12}$ as a result of the electron-electron repulsion. However, in this case this pattern is much more pronounced, and moreover, the distributions are in general much more located near the line $\theta_{13} = \theta_{12}$ which

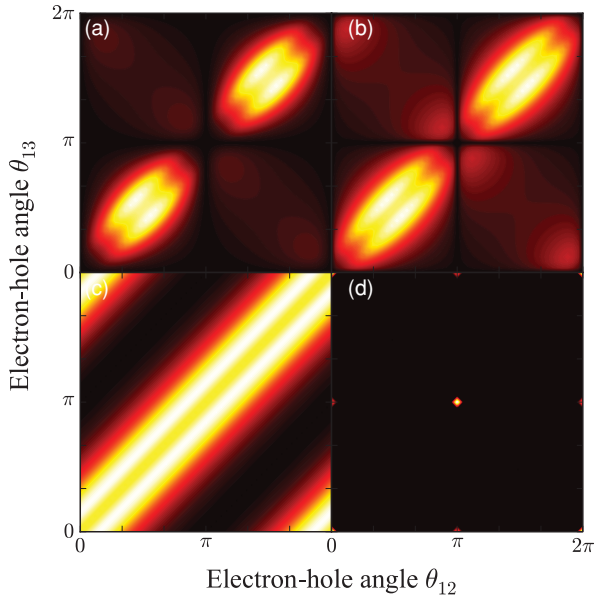

FIG. 9. (Color online) Probability distribution ρ_θ for the $S^+_{0.0}$ trion and θ_{13} for a) $D = 3.0$, b) $D = 2.5$, c) $D = 2.0$, and d) $D = 1.7$. In comparison with Fig. 8 these distributions are much more localized near the line $\theta_{13} = \theta_{12}$.

serves to lower the average angle difference $\langle S^+_{0.0}|\theta_{23}|S^+_{0.0}\rangle$ as is also seen in Fig. 5.

The binding energies presented up until this point are all expressed in universal units, i.e., in units of effective Rydberg Ry^* and effective Bohr radii a^*_B. This means that they can be applied to any system for which the dielectric constant and the effective electron- and hole masses are known. Examples of such systems are, amongst others, quantum wells[12–16] and nanotubes.[19] To guide experimentalists to the actual trion energies E_T for different systems we here give curve fits for $S^-_{0.0}$, $S^+_{0.2}$, $S^+_{0.0}$, and $S^{+/-}_{1.0}$. The trion binding energies can be approximated by

$$E^{+/-}_\sigma(D) = c_0 + \sum_{i=1}^{4} c_i D^{-i} e^{-D}, \tag{18}$$

with the coefficients given in Table I.

It is worth noting that the general concept of trions covers a very large variety of particles. These results would be applicable in the description of, for instance, impurity bound excitons[43] D^-, along with other applications as we will see in the next section.

TABLE I. Fitting coefficients – all in units of Ry^* – for the ground state energy of trions in Eq. (18) for $S^-_{0.0}$, $S^+_{0.0}$ and $S^{+/-}_{1.0}$.

	c_0	c_1	c_2	c_3	c_4
$E^-_{0.0}$	−0.765	368	−2390	4920	−3650
$E^+_{0.0}$	−0.751	262	−1680	3320	−2560
$E^+_{0.2}$	−0.563	212	−1570	3440	−2780
$E^{+/-}_{1.0}$	−0.420	158	−1330	3113	−2640

V. APPLICATIONS

To demonstrate how this model can be applied to real physical systems, and to stress the wide applicability of the results given above we study three systems in the following. First, we apply the method to the hydrogen molecular ion, which essentially is a $S^+_{0.0}$ trion. Then we turn our attention to trions in GaAs-based quantum wells and finally, we study the trions in CNTs.

A. Hydrogen molecular ion

For the hydrogen molecular ion the effective Rydberg is $Ry^* = \frac{1}{2}$Ha and the effective Bohr radius $a^*_B = 1a_B$ with Ha and a_B being the Hartree and the Bohr radius, respectively, defined as $\text{Ha} = \hbar^2/(m_e a_B^2)$ and $a_B = 4\pi\varepsilon_0\hbar^2/(m_0 e^2)$ in terms of the permittivity of free space ε_0, Planck's constant $\hbar$, the speed of light in vacuum c, and the free-electron mass m_0.

In three dimensional space the energy of the $S^+_{0.0}$ trion is found to be $E \approx 1.15Ry^* = 0.575\,\text{Ha}$ using Eq. (18). The expectation value $\langle S^+_{0.0}|r_{23}|S^+_{0.0}\rangle$ is $\langle S^+_{0.0}|r_{23}|S^+_{0.0}\rangle \approx 1.87a^*_B = 1.87a_B$ (Fig. 5). This should be compared with the exact energy 0.6Ha and proton-separation distance $2.0a_B$ in Ref. 44 which clearly demonstrates a good agreement.

The hydrogen molecular ion has also been studied in two dimensions in Ref. 44. If one takes $D = 2$ and redoes the above calculation it is found that $E \approx 5.37Ry^* = 2.68\,\text{Ha}$ and $\langle S^+_{0.0}|r_{23}|S^+_{0.0}\rangle = 0.62a_B$, and again we see a decent agreement with the exact values 2.823 Ha and $0.511a_B$ reported in Ref. 44.

In conclusion, this model predicts the energy and proton-separation distance with good precision. Clearly the inaccuracies could be overcome by extending the method presented here using either diffusion Monte Carlo or by using a basis expansion as done in Ref. 19.

B. Trions in GaAs quantum wells

Intuitively, a quantum well resembles a fractional dimensional system where particles are free to move in the (x, y)-plane while being confined in the z-direction. To account for the confinement in the z-direction it has been suggested that the dimension can be determined by considering the envelope functions of the electron and the hole. For infinite quantum wells it has been demonstrated that the effective dimension of the well can be estimated as[45]

$$D = 3 - e^{-\beta}. \tag{19}$$

The parameter $\beta = L/d$ is the ratio between the width of the well L, and the characteristic relative electron-hole separation.[45] If one considers the solutions to the infinite quantum well, β can be determined analytically. However, it is clear that with well barriers of typically a few hundred meV, GaAs quantum wells are far from being infinite barrier structures. For excitons a characteristic electron-hole separation of $d = 2a^*_B$ has shown to be quite accurate in comparison with other theoretical works.[45] For trions, however, d must be expected to be slightly larger due to the trion nature as an exciton with a weakly-bound electron. By fitting d to the theoretical works in

Ref. 46, we found that $d = 2.15a_B^*$ produces accurate results for trions. Thus, the parameters $\beta(L)$ are given by

$$\beta_X(L) = \frac{L}{2} \text{ and } \beta_T(L) = \frac{L}{2.15}, \tag{20}$$

for the exciton and the trion, respectively. Excitons in quantum wells now can be modelled by the expression[45]

$$E_X(L) = -\frac{4}{(2 - e^{-\beta_X})^2}, \tag{21}$$

whereas trions in general follow

$$E_\sigma^{+/-}(L) = c_0 + \sum_{i=1}^{4} c_i \left(3 - e^{-\beta_T}\right)^{-i} \exp\left(3 - e^{-\beta_T}\right), \tag{22}$$

with the coefficients given in Table I.

For GaAs the dielectric constant, and the effective electron- and hole masses are[46] $\varepsilon = 12.58$, $m_e = 0.067$, and $m_h = 0.34$, respectively. This gives a mass fraction of $\sigma \approx 0.2$, an effective exciton Rydberg of $Ry^* = 4.8\,\text{meV}$ and an effective Bohr radius of $a_B^* = 119\,\text{Å}$. Using these parameters, we first studied the negative trion in GaAs quantum wells. One can assume that the energies of S_σ^- can be approximated by the energy of the $S_{0.0}^-$ trion. This can be justified by investigating the mass fraction spectrum for various dimensions from which one will discover that this approximation will at most yield an error of 7%. Thus, one would expect that S_σ^- trions in quantum wells are well described by $E_{0.0}^-(L)$ given by Eq. (22). We have plotted this result in Fig. 10 along with the theoretical results reported in Ref. 46. Although it is seen that there is a good overall agreement between the two models the slope of the curves are somewhat different. This, however, is not so surprising as (1) the results in Ref. 46 are based upon a model with a finite well height, and (2) the mapping between the dimension and well-width Eq. (19) may be inaccurate.

Similarly for $\sigma \approx 0.2$, using Eq. (22) the $S_{0.2}^+$ trion binding energy was estimated for various well widths which is given in Fig. 10. We have also provided the experimentally observed

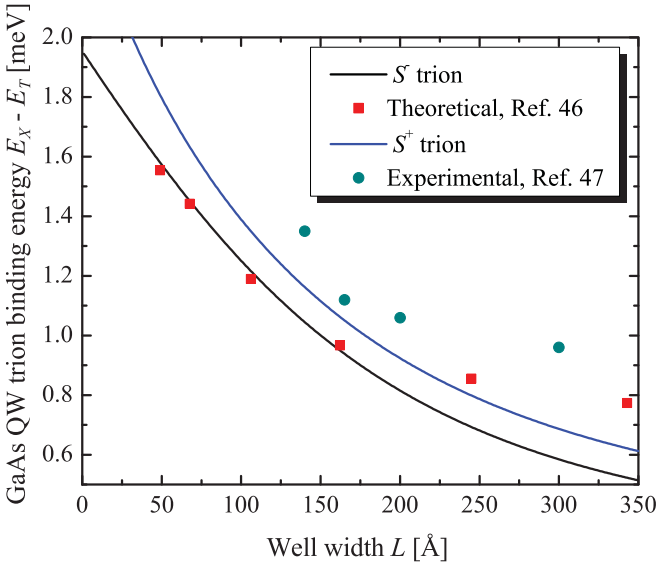

FIG. 10. (Color online) Trion binding energy in GaAs-based quantum wells for the positive and negative trion.

values from Ref. 47. As seen there is a reasonable agreement between values reported in Ref. 47 and our estimates. One should keep in mind, though, that our variational estimate underestimates the energy for the $S_{0.2}^+$ (Fig. 3), which explains why the experimentally found energies are slightly larger. Overall, the fractional dimensional theory models GaAs-based quantum wells to a satisfactory accuracy given the inherent limitations.

C. Trions in carbon nanotubes

Excitonic complexes in CNTs have been studied using many different approaches.[19,20,48–56] In Ref. 19 it was demonstrated that the fractional dimensional model predicts the trion binding energy in CNTs with very high accuracy and therefore we use this as an example. For CNTs the mass fraction is near[20,52] $\sigma \approx 1$. Along the same lines as Refs. 19 and 20, we first found the CNT effective Rydberg $Ry^* = 13.6\,\text{eV} \cdot \mu/\varepsilon^2$, where $\mu = m_e m_h/(m_e + m_h)$ is the reduced electron-hole mass in units of the free-electron mass m_0, and m_e and m_h are the effective electron and hole masses, respectively. Using a nearest neighbor tight-binding model[57] with a hopping integral[19] of $t = 2.89\,\text{eV}$ and an overlap integral of $s = 0.1$, the reduced electron and hole masses could be estimated from the CNT band structure. These parameters are considered reasonable as they predict the Fermi velocity in graphene to $v_F = 9.6 \times 10^5$ which is within 5.7% of the average experimental value.[58] As the band structures of CNTs are derived from that of graphene the errors of the estimated effective CNT masses are found within a similar error. The dielectric screening ε is determined partly by the CNTs themselves and partly by the surrounding material. By considering the contributions from each, one can argue[20] that the main contribution to the dielectric constant arises from the surrounding material and moreover, that the value of ε should be taken to be somewhere between[20,53,54] 2.0 and 5.0.

For example, we consider the (7,5) CNTs. In lack of a more precise value, we found ε by fitting the trion binding energies for CNTs where $2n + m = 20$ to experimental observed trion binding energies. We found that $\varepsilon = 3.4$ give precise results for these CNT species and will therefore use this value in the following. The effective electron and hole masses for (7,5) CNTs are then found as $m_e = 0.081m_0$ and $m_h = 0.087m_0$, giving a reduced mass $\mu = 0.042m_0$. Using this the effective Rydberg is $Ry^* \approx 49\,\text{meV}$. The dimension of CNTs has been shown to be[21] $D \approx 1.71$, for which the trion binding energy is $E_X - E_T = 1.27Ry^* \approx 63\,\text{meV}$. For tube diameters near 0.8 nm the exciton singlet-triplet splitting[59] is ≈110 meV and if this is taken into account the measured trion binding energy in Ref. 33 is found to be $170\,\text{meV} - 110\,\text{meV} = 60\,\text{meV}$ giving an error of 5%. We did this calculation for a wide variety of CNTs with diameters ranging from 0.5nm to 1.5nm. The result can be seen in Fig. 11. We have also plotted the experimentally observed values, where we have subtracted the exciton singlet-triplet splitting as explained in Ref. 33. In general, we find an extremely good agreement between the experimentally observed trion binding energies and the calculation done here for chiral indicies where $2n + m < 22$. However, for nanotubes where $2n + m$ is greater than 22, the agreement is not as convincing. This can be ascribed to

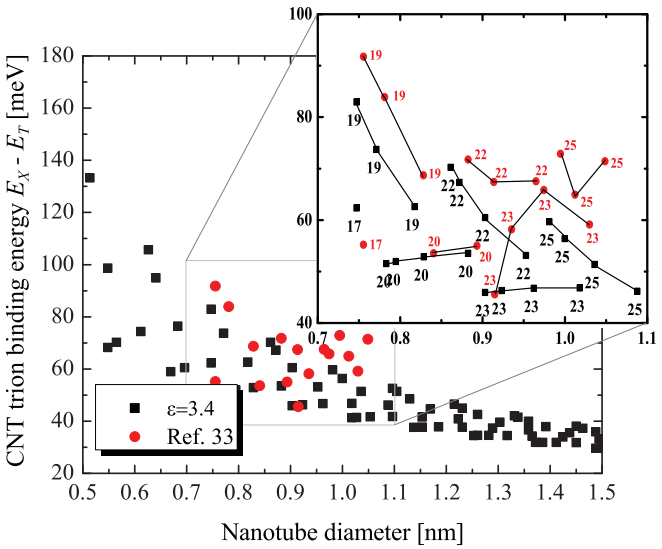

FIG. 11. (Color online) Comparison between calculated trion binding energies (black squares) and experimentally observed values (red circles). The energies were calculated by assuming that CNTs effectively are 1.71 dimensional nano structures[19] and assuming that[20] $E_\sigma^+ \approx E_{1.0}^{+/-}$. The effective energies were then converted into physical energies by calculating the effective Ry^*, as explained in the text, using a nearest neighbor tight binding model.

several factors. First of all, the singlet-triplet splitting[33,59] has been found experimentally and fitted to $70\,\text{meV} \times \text{nm}^2/d^2$ for nano tubes with diameter d given in nm. It is clear that such a fit might contain inaccuracies because of statistical uncertainty of the experimental measurements. Secondly, it should be stressed that the parameter $\varepsilon = 3.4$ is used as a fitting parameter because no precise value of ε is known for the species in Ref. 33. Within the model presented here ε has two effects on spectrum: (1) it shifts the binding energy toward zero as ε is increased, and (2) the broadening of the Kataura plot becomes more significant as ε is decreased. In a more accurate model, however, it is very likely that ε will differ for different CNTs and samples. Consequently, this might shift the trion energy significantly for the individual chiralities since $Ry^* \propto \varepsilon^{-2}$. Third, we use a fixed effective dimension of $D = 1.71$ which is an approximation. However, these results do confirm that it is very likely that results reported in Ref. 33 indeed do arise from trions.

VI. CONCLUSIONS

In this work we have investigated excitons and trions in fractional dimensional spaces. We have applied the Palmer model to obtain result equivalent to chose reported using the Herrick-Stillinger model. Because the interpolation between dimensions our results are valid for a wide range of geometries. We have explained the difficulties that occur when implementing VQMC in fractional dimensional spaces and suggested solutions to these problems. Also, we have shown that the general physics of the trion can be well estimated by a fairly simple trial function. We have brought additional information on the binding energy of the positive trion and explained the major differences of the positive and negative trion. Finally, we have applied this model to three systems which has demonstrated a good agreement with experimental- and theoretical works by other groups.

ACKNOWLEDGMENTS

T. F. Rønnow would like to thank Ulf G. Rønnow for his assistance with development of Maple routines as well as thank professor Francois M. Peeters, and his group, for their hospitality.

APPENDIX A: PALMER- AND HERRICK-STILLINGER MODELS

In this section we review the Palmer model, and using the results in Refs. 23 and 24 we establish an expression for the integration measure used in this paper. We also explain the relation between the Palmer- and Herrick-Stillinger model, and demonstrate that the Herrick-Stillinger model is contained within the Palmer model. In the Palmer model, the integration measure is given by[23]

$$dx = \prod_{i=1}^{3N} d^{\alpha_i} x_i, \quad d^{\alpha_i} x_i = \sigma(\alpha)|x_i|^{\alpha_i - 1} dx_i, \tag{A1}$$

$$\sigma(\alpha) = \frac{\pi^{\alpha/2}}{\Gamma\left(\frac{\alpha}{2}\right)}, \tag{A2}$$

where $x \in \mathbb{R}^{3N}$ denotes the position in the fractional dimensional space, x_i denotes the component along the i'th axis and $\alpha_i \in [0,1]$ is a parameter used to control the "collapse" of the axis. It is easily demonstrated that

$$\lim_{\alpha_i \to 1} d^{\alpha_i} x_i = \lim_{\alpha_i \to 1} |x_i|^{\alpha_i - 1} dx_i = dx_i, \tag{A3}$$

and

$$\lim_{\alpha_i \to 0} d^{\alpha_i} x_i = \lim_{\alpha_i \to 0} \tfrac{1}{2}\alpha_i |x_i|^{\alpha_i - 1} dx_i = \delta(x_i) dx_i, \tag{A4}$$

which provides us with an immediate understanding of the limiting cases: In the first case $\alpha_i \to 1$ integration along the i'th axis corresponds to integration over the set of reals $\mathbb{R}$. In the latter case $\alpha_i \to 0$, the integration weight becomes a Dirac delta function, and so, the integration corresponds to evaluating the function in $x_i = 0$. This is also what we would expect as it is the only intuitive way of performing a "collapse" of an axis. The infinitesimal D dimensional volume element in Eq. (A1) directly gives

$$\int f(x)dx = \sigma^N(\alpha)\sigma^N(\beta)\sigma^N(\gamma) \int_{-\infty}^{\infty} \cdots \int_{-\infty}^{\infty} f(\vec{r}_1, \ldots, \vec{r}_N) \times \prod_{i=1}^{N} |x_i|^{\alpha-1} |y_i|^{\beta-1} |z_i|^{\gamma-1} dx_i dy_i dz_i, \tag{A5}$$

where x is an element in $\mathbb{R}^{3N}$, $\vec{r}_i = \langle x_i, y_i, z_i \rangle$ in $\mathbb{R}^3$ denotes the position of the i'th particle, and we have introduced α, β, and γ to control the collapse of the x-, y-, and z-axes, respectively. We define the dimension D as the sum of the individual collapse parameters $D = \alpha + \beta + \gamma$.

The relation between the integration in Eq. (2) and the one developed by Herrick and Stillinger, can be found by

introducing radial coordinates[24]

$$\begin{aligned} x_1 &= r_1 \cos\theta_1, \\ y_1 &= r_1 \sin\theta_1 \cos\phi_1, \\ z_1 &= r_1 \sin\theta_1 \sin\phi_1, \\ x_2 &= r_2 \cos\theta_2, \\ &\vdots \\ z_N &= r_N \sin\theta_N \sin\phi_N, \end{aligned} \tag{A6}$$

along with calculating the corresponding Jacobian[23]

$$J_{3N} = r_1^2 \sin\theta_1 r_2^2 \sin\theta_2 \ldots r_N^2 \sin\theta_N, \tag{A7}$$

to show that the integral of $f(x)$ in fractional dimensional space for N particles can be expressed as

$$\begin{aligned} \int f(x)dx &= \sigma^N(\alpha)\sigma^N(\beta)\sigma^N(\gamma) \\ &\times \int \ldots \int f(r_1,\theta_1,\phi_1,r_2,\ldots,\phi_N) \\ &\times \prod_j^N r_j^{\alpha+\beta+\gamma-1} |\cos\theta_j|^{\alpha-1} |\sin\theta_j|^{\beta+\gamma-1} \\ &\times |\cos\phi_j|^{\beta-1} |\sin\phi_j|^{\gamma-1} dr_j d\theta_j d\phi_j. \end{aligned} \tag{A8}$$

If one now takes[23] $\alpha = 1$, defines $D = 1 + \beta + \gamma$, and assumes that $f(x)$ is independent of ϕ one arrives at the Herrick-Stillinger integration

$$\begin{aligned} \int f(x)dx &= \sigma^N(D-1) \\ &\times \int_0^\infty \int_0^{2\pi} \ldots \int_0^\infty \int_0^{2\pi} f(r_1,\theta_1,\ldots,r_N,\theta_N) \\ &\times \prod_j^N r_j^{D-1} |\sin\theta_j|^{D-2} dr_j d\theta_j. \end{aligned} \tag{A9}$$

The Laplacian derived from the Palmer model can also be shown to be similar to that of Herrick and Stillinger.[23]

*tfr@nanophysics.dk; http://www.nanophysics.dk
†tgp@nano.aau.dk
‡bart.partoens@ua.ac.be
§kkb@math.aau.dk

[1] C. Palmer, J. Phys. A: Math. Gen. **37**, 6987 (2004).
[2] D. R. Herrick and F. Stillinger, Phys. Rev. A **11**, 42 (1975).
[3] P. K. Basu, *Theory of optical processes in semiconductors* (Oxford Science Publications, 2005).
[4] G. Bastard, E. E. Mendez, L. L. Chang, and L. Esaki, Phys. Rev. B **26**, 1974 (1982).
[5] T. Ando, J. Phys. Soc. Jpn. **66**, 1066 (1997).
[6] C. D. Spataru, S. Ismail-Beigi, L. X. Benedict, and S. G. Louie, Phys. Rev. Lett. **92**, 077402 (2004).
[7] A. Thilagam, Phys. Rev. B **56**, 4665 (1997).
[8] X. F. He, Phys. Rev. B **43**, 2063 (1991).
[9] T. G. Pedersen, Carbon **42**, 1007 (2004).
[10] J. R. Guest, T. H. Stievater, X. Li, J. Cheng, D. G. Steel, D. Gammon, D. S. Katzer, D. Park, C. Ell, A. Thränhardt, G. Khitrova, and H. M. Gibbs, Phys. Rev. B **65**, 241310 (2002).
[11] F. Wang, G. Dukovic, L. E. Brus, and T. F. Heinz, Science **308**, 838 (2005).
[12] J. Singh, D. Birkedal, V. G. Lyssenko, and J. M. Hvam, Phys. Rev. B **53**, 15909 (1996).
[13] Z. P. Wang and X. X. Liang, Solid State Commun. **150**, 356 (2010).
[14] A. Matos-Abiague, J. Phys. Condens. Matter **14**, 4543 (2002).
[15] R. Escorcia, J. Sierraortega, I. Mikhailov, and F. Betancur, Physica B **355**, 255 (2005).
[16] M. de Dios-Leyva, A. Bruno-Alfonso, A. Matos-Abiague, and L. E. Oliveira, J. Appl. Phys. **82**, 3155 (1997).
[17] D. R. Herrick and F. H. Stillinger, Phys. Rev. A **11**, 42 (1975).
[18] F. H. Stillinger, J. Math. Phys. **18**, 1224 (1977).
[19] T. F. Rønnow, T. G. Pedersen, and H. D. Cornean, J. Phys. A **43**, 474031 (2010).
[20] T. F. Rønnow, T. G. Pedersen, and H. D. Cornean, Phys. Rev. B **81**, 205446 (2010).
[21] T. G. Pedersen. Solid State Commun. **141**, 569 (2007).
[22] D. A. Kleinman, Phys. Rev. B **28**, 871 (1983).
[23] C. Palmer and P. N. Stavrinou, J. Phys. A **37**, 6987 (2004).
[24] M. Sadallah and S. I. Muslih, Int. J. Theor. Phys. **48**, 3312 (2009).
[25] J. Kundrotas, A. Cerskus, S. Asmontas, G. Valusis, B. Sherliker, M. P. Halsall, M. J. Steer, E. Johannessen, and P. Harrison, Phys. Rev. B **72**, 235322 (2005).
[26] M. Sadallah, S. Muslih, and D. Baleanu, Czech. J. Phys. **56**, 323 (2006).
[27] S. Muslih, D. Baleanu, and E. Rabei, Cent. Eur. J. Phys. **5**, 285 (2007).
[28] S. Muslih, D. Baleanu, and E. Rabei, Cent. Eur. J. Phys. **5**, 549 (2007).
[29] A. C. Cancio and Y. C. Chang, Phys. Rev. B **47**, 13246 (1993).
[30] R. W. Hall and P. G. Wolynes, Phys. Rev. B **33**, 7879 (1986).
[31] E. A. Burovski, A. S. Mishchenko, N. V. Prokof'ev, and B. V. Svistunov, Phys. Rev. Lett. **87**, 186402 (2001).
[32] J. Thijssen, *Computational Physics* (Cambridge University Press, 2007).
[33] R. Matsunaga, K. Matsuda, and Y. Kanemitsu, Phys. Rev. Lett. **106**, 037404 (2011).
[34] J. P. Dahl, *Introduction to the quantum world of atoms and molecules* (World Scientific, Singapore, 2005).
[35] We have not shown an explicit expression for the local energy here as it is rather complicated though trivial to derive.
[36] T. P. Straatsma, H. J. C. Berendsen, and A. J. Stam, Mol. Phys. **57**, 89 (1986).
[37] It is constant up to a factor of two in the region $[0.2,1.2]a_B^*$.
[38] A. Harju, B. Barbiellini, S. Siljamäki, R. M. Nieminen, and G. Ortiz, Phys. Rev. Lett. **79**, 1173 (1997).
[39] X. Lin, H. Zhang, and A. M. Rappe, J. Chem. Phys. **112**, 2650 (2000).
[40] This is only true for three-particles. For four particles one will need at least 3 parameters.

[41]Note that this angle is in the interval $[0,\pi]$, and *not* $[0,2\pi]$ as it is the angle between two vectors. If one naively takes $\theta_{23} = |\theta_{13} - \theta_{12}|$ or even $\theta_{23} = \theta_{13} - \theta_{12}$, the obtained result does not have any physical meaning.
[42]This can be verified numerically.
[43]P. Tronc and V. P. Smirnov, Phys. Rev. B **66**, 165223 (2002).
[44]J.-L. Zhu and J.-J. Xiong, Phys. Rev. B **41**, 12274 (1990).
[45]H. Mathieu, P. Lefebvre, and P. Christol, Phys. Rev. B **46**, 4092 (1992).
[46]A. V. Filinov, C. Riva, F. M. Peeters, Yu. E. Lozovik, and M. Bonitz, Phys. Rev. B **70**, 035323 (2004).
[47]J. L. Osborne, A. J. Shields, M. Pepper, F. M. Bolton, and D. A. Ritchie, Phys. Rev. B **53**, 13002 (1996).
[48]H. D. Cornean, P. Duclos, and B. Ricaud, Ann. Inst. Henri Poincare **8**, 135 (2007).
[49]H. D. Cornean, P. Duclos, and B. Ricaud, Few-Body Syst. **38**, 125 (2006).
[50]T. F. Rønnow, T. G. Pedersen, and H. D. Cornean, Phys. Lett. A **373**, 1478 (2009).
[51]H. D. Cornean, P. Duclos, and T. G. Pedersen, Few-Body Syst. **34**, 155 (2004).
[52]T. G. Pedersen, Phys. Rev. B **67**, 073401 (2003).
[53]T. G. Pedersen, K. Pedersen, H. D. Cornean, and P. Duclos, Nano Lett. **5**, 291 (2005).
[54]D. Kammerlander, D. Prezzi, G. Goldoni, E. Molinari, and U. Hohenester, Phys. Rev. Lett. **99**, 126806 (2007).
[55]I. V. Bondarev, Phys. Rev. B **83**, 153409 (2011).
[56]K. Watanabe and K. Asano, Phys. Rev. B **83**, 115406 (2011).
[57]R. Saito, G. Dresselhaus, and M. S. Dresselhaus, *Physical Properties of Carbon Nanotubes* (Imperial College Press, 2003).
[58]A. Grüneis, C. Attaccalite, L. Wirtz, H. Shiozawa, R. Saito, T. Pichler, and A. Rubio, Phys. Rev. B **78**, 205425 (2008).
[59]R. Matsunaga, K. Matsuda, and Y. Kanemitsu, Phys. Rev. B **81**, 033401 (2010).